Tunable graphene system with two decoupled monolayers

H. Schmidt, T. Lüdtke, P. Barthold, E. McCann, V. I. Fal'ko, and R. J. Haug

Tunable graphene system with two decoupled monolayers

H. Schmidt,[1,a] T. Lüdtke,[1] P. Barthold,[1] E. McCann,[2] V. I. Fal'ko,[2] and R. J. Haug[1]

[1]*Institut für Festkörperphysik, Leibniz Universität Hannover, Appelstr. 2, 30167 Hannover, Germany*
[2]*Department of Physics, Lancaster University, Lancaster LA1 4YB, United Kingdom*

The use of two truly two-dimensional gapless semiconductors, monolayer and bilayer graphene, as current-carrying components in field-effect transistors (FETs) gives access to special types of nanoelectronic devices. Here, we report on the development of graphene-based FETs containing two decoupled graphene monolayers manufactured from a single one folded during the exfoliation process. The transport characteristics of these devices differ markedly from those manufactured from a single-crystal bilayer. By analyzing Shubnikov–de Haas oscillations, we demonstrate the possibility to independently control the carrier densities in both layers using top and bottom gates, despite there being only a nanometer scale separation between them. © *2008 American Institute of Physics.* [DOI: 10.1063/1.3012369]

The development of the micromechanical cleavage technique for manufacturing ultrathin graphitic films has made it possible to produce field-effect transistors (FETs) based on monolayer graphene and to study their electronic properties,[1–4] indicating that graphene is a gapless semiconductor with a peculiar Dirac-type spectrum of charge carriers. Using micromechanical exfoliation, multilayers of graphene are also often produced. Two layers of graphene prepared by exfoliation usually exhibit crystalline ordering with a characteristic AB stacking,[5,6] later referred to as single-crystal (SC) bilayer. This should be contrasted to pairs/stacks of individual misoriented graphene flakes identified among some of the peeled graphitic films using Raman spectroscopy[7] and in multilayers grown epitaxially on silicon carbide.[8] While the individual carrier density in such layers is usually beyond experimental control, in this paper we report on the realization of two-layer graphene-based FETs where the density on the two monolayers can be varied separately, despite them lying only a dozen angstroms apart.

The nanostructures presented in this Letter were prepared by peeling off pieces from natural bulk graphite[9] with adhesive tape and placing them on a silicon wafer covered with SiO$_2$. Since at the intermediate stage of the utilized deposition process only some part of the graphene flake touches the SiO$_2$ surface, the flake flips over during the removal of the adhesive tape, thus producing two misoriented graphene layers lying on top of each other and separated by occasional surface deposits [Fig. 1(a) sketches the top view of such a structure]. Then, this material is processed into Hall-bar samples using plasma etching and contacted (to both layers) by evaporating chromium and gold electrodes [Fig. 1(b)]. Figure 2(a) shows two optical images of such a sample before and after plasma etching. A darker than other areas top-left edge indicates the position of the fold. Scanning the structure with an atomic force microscope (AFM) reveals a double step at the etched edges [Figs. 2(c) and 2(d)] with a first-step height of 1.1 nm. Although layers of graphene should have a height of 0.34 nm, previous AFM measurements showed values up to 1 nm for single layer graphene lying on a substrate[1] attributed to a water layer

underneath graphene and/or the rippling graphene surface. From these data and also from the transport measurements shown below we conclude that the first step is due to a monolayer of graphene. The second step has a height of 0.6 nm which is larger than the thickness of one layer but less than the height of two AB stacked layers. This indicates that the second layer is also a single layer which is separated further from the first layer than in a conventional bilayer.

To distinguish the designed device from monolayers or SC bilayers we performed transport measurements on the sample shown in Fig. 2, applying magnetic fields up to 13 T at temperatures down to 1.5 K. To reduce the influence of contact resistance on the measurements, a multiterminal device has been used, and different combinations of two and three point measurements were performed at a broad range of back-gate voltage, $-70 \text{ V} < V_{BG} < 70 \text{ V}$, applied between the substrate of n-Si and graphene. As usual, positive back-gate voltage induces electrons, negative holes. Figure 2(b) shows the measured field effect on graphene resistivity, demonstrating the operation of the device as a FET.[1] A characteristic peak in the observed resistivity points at the approximate neutrality condition for the graphene layers, which is shifted to a finite back-gate voltage $V_{BG}^0 = 11.5$ V, indicating natural doping of the graphene flakes. The measured maximum resistivity, $\rho_{max} \approx 3.3$ kΩ at 1.5 K, is about half of the earlier-reported typical values for monolayers,[2,4] which is in line with the assumption that the device consists of two monolayers conducting in parallel.

Most importantly, the layer structure of ultrathin graphitic films can be characterized by analyzing the Shubnikov–de Haas (SdH) oscillations in the flake resistance
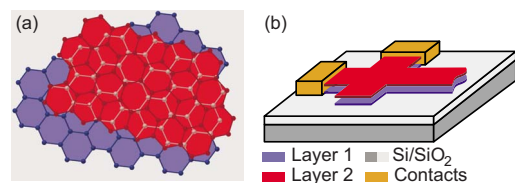

FIG. 1. (Color online) (a) Top view of a pair of arbitrarily oriented graphene monolayers (layer 2, red and layer 1, blue) in a two-layer stack. (b) A two-layer stack on top of a Si/SiO$_2$ (gray/light gray) wafer, etched and contacted (yellow) for transport measurements.

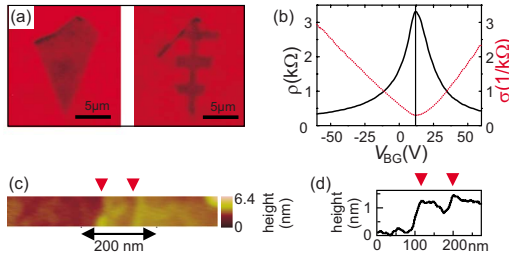[a]Electronic mail: h.schmidt@nano.uni-hannover.de.

FIG. 2. (Color online) (a) Optical image of the two-layer sample before and after etching. (b) The resistivity (black) and the conductivity (red dots) plotted vs the back-gate voltage applied between silicon substrate and graphene. (c) The AFM image of the edge showing two steps (red arrows) and (d) its averaged height profile.

$R(B)$ studied as a function of a magnetic field B applied perpendicular to the sample. Berry's phase π characteristic of electrons in monolayer graphene is directly related to the appearance of SdH oscillations minima at filling factors $\nu_{min}=4(i+1/2)$,[2,3] in contrast to SC bilayer graphene[6] where electron's Berry's phase is 2π and the SdH oscillation minima appear at filling factors $\nu_{min}=4i$, with $\nu=nh/eB$ being the filling factor, n the carrier concentration, and i an integer. When studied at a fixed back-gate voltage [e.g., $V_{BG}=-70$ V and $V_{BG}=-40$ V, Figs. 3(a) and 3(b)], the magnetoresistance measured in the two-layer device and plotted versus $1/B$ displays oscillations with two very different periods [compared in detail in the top/bottom panels of Figs. 3(a) and 3(b)], manifesting the coexistence of two very different carrier densities, n_1 and n_2, in the sample. These two density values can be obtained from the period ΔB^{-1} of the SdH oscillations as $n=4e/h\Delta B^{-1}$ (where we take into account both the spin and valley degeneracy in the graphene band structure). Their experimentally determined gate-voltage dependence is shown in Fig. 3(d). Systematically repeated at all the studied voltage values, the periodicity of both fast (lower panel) and slow (upper panel) $1/B$ oscilla-
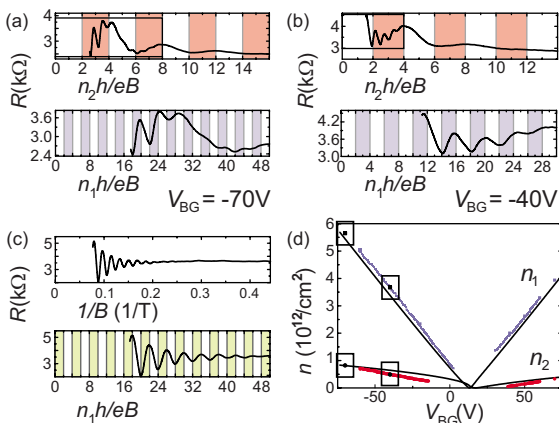

FIG. 3. (Color online) (a) Longitudinal resistance measured as a function of a perpendicular magnetic field for $V_{BG}=-70$ V. The upper figure shows the oscillation corresponding to the lower carrier concentration n_2; the zoomed part in the bottom panel shows the oscillations corresponding to the high concentration, n_1. (b) Same plots for $V_{BG}=-40$ V. (c) Comparable measurement on a SC bilayer showing only one sequence of oscillations with typical bilayer behavior. (d) Two carrier concentrations in the two-layer (folded) graphene sample extracted from the period of the SdH oscillations. The boxes mark the points obtained using the data shown in panels (a) and (b). The black lines are the results of the theoretical modeling of the device. A shift in the gate voltage of 11.5 V takes into account doping of graphene by deposits.

tions in the two-layer structure was such that the resistivity minima could only be attributed to the sequence of filling factors $\nu_{min}=4(i+1/2)$, which is typical for monolayer graphene. To highlight this behavior of the presented data, in the top/bottom panels of Figs. 3(a) and 3(b) the $1/B$ intervals with the rising parts of the corresponding oscillations are colored. For comparison, Fig. 3(c) shows the results of a similar study performed for a SC bilayer, where the sequencing of the SdH oscillation minima coincides with the earlier observed[5] appearance of maxima at filling factors $\nu_{min}=4i$ specific for such a material. Finally, the observed carrier densities n_1 and n_2 in the two-layer device and their dependence on back-gate voltage presented in Fig. 3(d) can be compared to theoretically calculated values plotted on the same figure as lines. The presented calculation takes into account the electrostatics of the device containing two monolayers at distance $d\approx 1.5$ nm from each other lying on top of the SiO_2 dielectric layer (with permittivity $\epsilon_b=3.9$ and thickness L_{BG}), Fermi-energy dependence of the compressibility of the electron gas with the Dirac spectrum $E(p)=vp$, and additional doping charge, $\delta n \approx 2 \times 10^{11}$ cm^{-2} due to deposits left on top of the upper layer in the course of the manufacturing process. The parameters used in this calculation were obtained by fitting the observed V_{BG} dependence with the analytical result relating the two densities on two parallel graphene flakes,

$$2\sqrt{\pi}d(e^2/\epsilon_0)[n_2 + \delta n] = hv(s_1\sqrt{|n_1|} - s_2\sqrt{|n_2|}), \quad (1)$$

$$n_1 + n_2 + \delta n = \frac{\epsilon_0 \epsilon_b V_{BG}}{e L_{BG}}, \quad (2)$$

where the first equation states the equivalence of the electrochemical potentials on the two graphene layers with $s_i=n_i/|n_i|$, whereas the second relates the total charge density in the device to its electrostatic capacity.

To tune the two carrier densities independently on the two parallel layers, we fabricated a two-layer sample with an additional top gate. A schematic view of the manufactured device is shown in Fig. 4(a), with the design resembling that of the top-gated SC bilayer structures used recently.[10] To fabricate the top gate, polymethylmethacrylate (PMMA) was spun onto a Hall-bar device which was produced in a similar way as the sample shown in Fig. 2. The PMMA layer was partially exposed to an electron beam converting the PMMA into a layer insoluble by acetone. Putting the sample in an acetone bath leaves an insulating PMMA layer of about 60 nm on top of the graphene flake. A local top gate with an area of 2.5 μm^2 was fabricated on top of this PMMA layer using standard electron beam lithography. Figure 4(b) shows an image of the top-gated sample. The resistance measured in this device as a function of the back-gate voltage for a fixed top-gate voltage, V_{TG} is shown in Fig. 4(c) (for $V_{TG}=15$ V). Its back-gate voltage dependence contains two pronounced peaks (marked by arrows), indicating the difference between the carrier concentrations in the top-gated and free parts of the device. The back-gate voltage interval between the two peaks corresponds to the bipolar transistor regime, with a p-n-p junction[11] formed underneath the top gate.[12,13] The tunability of the device using the top gate is demonstrated in Fig. 4(d). Here, the back-gate voltage was kept fixed at $V_{BG}=-40$ V and the top-gate voltage, V_{TG}, was varied. Due to the large negative back-gate voltage, the resis-
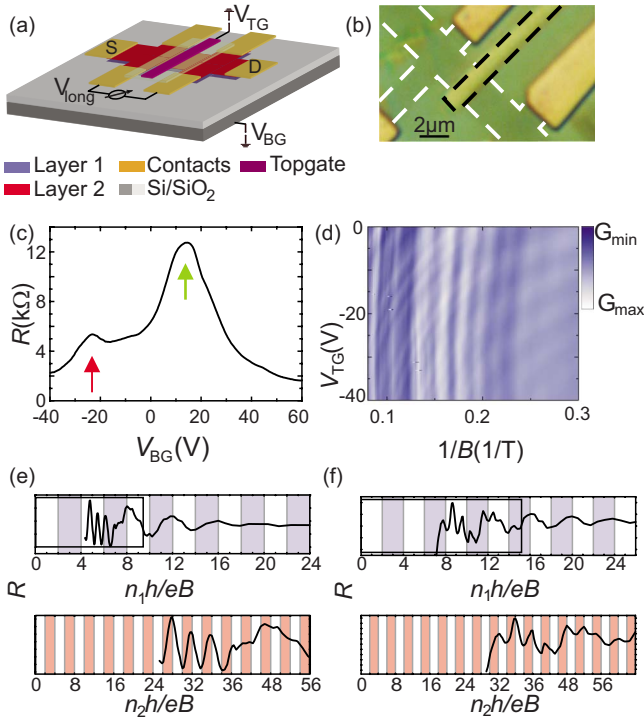
FIG. 4. (Color online) (a) Schematic of the second sample used in the experiment. The graphene layer and the top-gate metallic plate are separated via a PMMA layer. A current I was driven through the source-drain contacts (yellow) while the longitudinal resistance (R) was measured. The two layers are marked in red (layer 2) and blue (layer 1). (b) Image of the sample showing the etched flake, the contacts, and the top gate. The edges of the flake and of the top gate are highlighted using dashed lines. (c) Longitudinal resistance vs back-gate voltage for $V_{TG}=15$ V. The maxima in the resistance correspond to the two neutrality points underneath the top gate (red arrow) and outside the gated region (green arrow). Using the shift with gate voltages, one obtains a ratio of 2.5 between the capacitive couplings of the flake to the top and back gates. (d) Two-dimensional plot showing dR/dB vs the inverse magnetic field (B^{-1}) and the top-gate voltage at $V_{BG}=-40$ V. Different sets of SdH oscillations can be seen. Traces for two different top-gate voltages ($V_{TG}=-14$ V and $V_{TG}=-31$ V) are depicted in (e) and (f), showing maxima at $nh/eB=0$ for both oscillations.

tance maximum corresponding to the "neutrality point" in the top-gated region appears at positive voltage $V_{TG}=26$ V (not shown in the figure). To improve the visibility of the SdH oscillations and their evolution with V_{TG}, we differentiate the device's resistance with respect to the magnetic field value and show the result using the blue-scale plot in Fig. 4(d) where one sees several sets of oscillations. The oscillations which are almost independent of the top-gate voltage originate from the areas outside the top-gated region. The oscillations with a strong V_{TG} dependence characterize the layers underneath the top gate. The deconvolution of these two contributions is achieved by the numerical subtraction of the V_{TG} independent part of the resistance. The resulting magneto-oscillations are shown in Figs. 4(e) and 4(f) as function of filling factor for $V_{TG}=-14$ V and $V_{TG}=-31$ V. Similar to the first two-layer device, the top-gated structure shows the superposition of two monolayer-type SdH oscillations with different periods corresponding to densities

$n_2=6.32\times10^{12}$ cm^{-2} and $n_1=1.08\times10^{12}$ cm^{-2} for $V_{TG}=-14$ V and $V_{BG}=-40$ V and to $n_2=7.44\times10^{12}$ cm^{-2} and $n_1=1.80\times10^{12}$ cm^{-2} for $V_{TG}=-31$ V and $V_{BG}=-40$ V. This demonstrates not only that the different carrier densities on the two closely laid graphene layers can be detected but also that those densities can be independently controlled and tuned using a combination of top/back gates.

In conclusion, we demonstrated the realization of a graphene-based FET containing two decoupled graphene monolayers at a nanometer distance from each other. Using the magnetotransport measurements, we determine the carrier densities on the two parallel layers and show the ability to control those densities separately using a combination of electrostatic (back and top) gates. When operated in a broad voltage range, such a device could be employed in a search for the recently predicted superfluidity[14] in the "excitonic insulator" state expected to form in a pair of graphene layers with opposite polarity. Also, the technique of layer folding offers a promising method for making devices with separately contacted pairs of monolayers acting as atomically thin optically transparent[15,16] electrodes to study vertical transport and electro-optical characteristics of nanoparticles of various materials that can be captured between them.

[1] K. S. Novoselov, A. K. Geim, S. V. Morozov, D. Jiang, Y. Zhang, S. V. Dubonos, I. V. Grigorieva, and A. A. Firsov, Science **306**, 666 (2004).
[2] K. S. Novoselov, A. K. Geim, S. V. Morozov, D. Jiang, M. I. Katsnelson, I. V. Grigorieva, S. V. Dubonos, and A. A. Firsov, Nature (London) **438**, 197 (2005).
[3] Y. Zhang, Y. W. Tan, H. L. Stormer, and P. Kim, Nature (London) **438**, 201 (2005).
[4] A. K. Geim and K. S. Novoselov, Nature Mater. **6**, 183 (2007).
[5] K. S. Novoselov, E. McCann, S. V. Morozov, V. I. Fal'ko, M. I. Katsnelson, U. Zeitler, D. Jiang, F. Schedin, and A. K. Geim, Nat. Phys. **2**, 177 (2006).
[6] E. McCann and V. I. Fal'ko, Phys. Rev. Lett. **96**, 086805 (2006).
[7] P. Poncharal, A. Ayari, T. Michel, and J.-L. Sauvajol, Phys. Rev. B **78**, 113407 (2008).
[8] J. Hass, F. Varchon, J. E. Milla'n-Otoya, M. Sprinkle, N. Sharma, W. A. de Heer, C. Berger, P. N. First, L. Magaud, and E. H. Conrad, Phys. Rev. Lett. **100**, 125504 (2008).
[9] NGS Naturgraphit GmbH.
[10] J. B. Oostinga, H. B. Heersche, X. Liu, A. F. Morpurgo, and L. M. K. Vandersypen, Nature Mater. **7**, 151 (2008).
[11] V. V. Cheianov and V. I. Fal'ko, Phys. Rev. B **74**, 041403 (2006).
[12] B. Özyilmaz, P. Jarillo-Herrero, D. Efetov, D. A. Abanin, L. S. Levitov, and P. Kim, Phys. Rev. Lett. **99**, 166804 (2007).
[13] J. R. Williams, L. DiCarlo, and C. M. Marcus, Science **317**, 638 (2007).
[14] H. Min, R. Bistritzer, J.-J. Su, and A. H. MacDonald, Phys. Rev. B **78**, 121401 (2008).
[15] D. Abergel, A. Russell, and V. I. Fal'ko, Appl. Phys. Lett. **91**, 063125 (2007).
[16] R. R. Nair, P. Blake, A. N. Grigorenko, K. S. Novoselov, T. J. Booth, T. Stauber, N. M. R. Peres, and A. K. Geim, Science **320**, 1308 (2008).